Chinese Chemical Letters 33 (2022) 1325–1330

Contents lists available at ScienceDirect

Chinese Chemical Letters

journal homepage: www.elsevier.com/locate/cclet

Silicotungstic acid-derived WO_3 composited with ZrO_2 supported on SBA-15 as a highly efficient mesoporous solid acid catalyst for the alkenylation of *p*-xylene with phenylacetylene

Xueting Bai[1], Yongle Guo[1], Zhongkui Zhao*

State Key Laboratory of Fine Chemicals, Department of Catalysis Chemistry and Engineering, School of Chemical Engineering, Dalian University of Technology, Dalian 116024, China

ARTICLE INFO

Article history:
Received 9 April 2021
Revised 1 June 2021
Accepted 27 July 2021
Available online 5 August 2021

Keywords:
Alkenylation
SBA-15
Zirconium dioxide
Tungsten trioxide
Silicotungstic acid
Solid acid

ABSTRACT

Highly dispersed silicotungstic acid-derived WO_3 composited with ZrO_2 supported on SBA-15 (WZ/SBA-15) as an ordered mesoporous solid acid catalyst was prepared *via* a facile incipient wetness impregnation (IWI) method that active ingredients, ZrO_2 and WO_3, were impregnated into the channels of SBA-15 simultaneously with a subsequent calcination process. The relationship between catalyst nature and performance was explored by high resolution transmission electron microscopy (HRTEM), high-angle annular dark-field scanning transmission electron microscopy (HAADF-STEM), FT-IR, X-ray photoelectron spectroscopy (XPS), X-ray diffraction (XRD), N_2 adsorption-desorption, NH_3 temperature-programmed desorption (NH_3-TPD), and FT-IR of pyridine adsorption (Py-IR) characterization techniques. The catalytic performance of $W_{12}Z_{15}$/SBA-15 is not only greater than that of single component solid acid catalysts, WO_3/SBA-15 and ZrO_2/SBA-15, but also W_{12}/Z_{15}/SBA-15 prepared by impregnating active ingredients, ZrO_2 and WO_3, into SBA-15 in sequence. The outstanding performance of $W_{12}Z_{15}$/SBA-15 is derived from the strong interaction between ZrO_2 and WO_3, which results in more acid sites, and relatively high specific surface area, large pore volume, and ordered mesoporous structure of SBA-15. The characterization and reaction results clearly demonstrate that the synergy of ZrO_2 and WO_3 has a clear boost for the alkenylation. The optimized $W_{12}Z_{15}$/SBA-15-500 achieves a 99.4% conversion of phenylacetylene and a 92.3% selectivity of main product α-arylstyrene for the alkenylation of *p*-xylene with phenylacetylene, with very low level of oligomers producing at the same time. Moreover, $W_{12}Z_{15}$/SBA-15-500 shows excellent catalytic stability and regeneration. Therefore, $W_{12}Z_{15}$/SBA-15-500 is a promising solid acid catalyst for the alkenylation.

Alkenyl aromatics, synthesized by acid-catalyzed alkenylation of aromatic compounds with alkynes, especially solid acid catalysts in terms of its features of high efficiency, low-cost, clean, renewability, easy-separation, and applicability toward large-scale industrial continuous production [1–3], are widely applied to diverse fields such as flavors, dyes, natural products, pharmaceuticals, and agrochemicals [4–6]. Due to oligomerization of alkynes as the result of the poor stability of vinyl cation species [7], alkenylation remains a serious challenge to overcome. Compared with homogeneous catalysts, which leads to heavy pollution and equipment corrosion issues, heterogeneous catalysts, especially solid acid catalysts, show greater application potential for the alkenylation, whose acidity and pore structure have decisive effect on the catalytic activation, selectivity, and coke resistance. Therefore, it is urgent to develop highly efficient solid acid catalysts for alkenylation [8].

Some pioneering work has been done by Sartori who used HSZ-360 to catalyze the alkenylation of aromatics, which gave an unsatisfactory result owing to the existing irreconcilable contradiction between catalytic activity and selectivity. Besides, the use of HY zeolite to alkenylation contributed to a low catalytic efficiency, ascribed that the reaction only took place on the external surface of the catalyst as a result of the narrow pore channels within the HY zeolite [9]. Consequently, the mesoporous solid acid catalyst may be a wise choice for alkenylation. In our previous reports, a series of supported phosphotungstic acid mesoporous solid acid catalysts have been developed for alkenylation, but inevitable use of volatile organic solvent for the recovery of spent catalysts results in economic and environmental issues [10–12]. Besides, a series of sulphated La-mediated ZrO_2-based solid acid catalysts have been developed for the alkenylation [13–15], considering the superacidic

* Corresponding author.
E-mail address: zkzhao@dlut.edu.cn (Z. Zhao).
[1] These authors contributed equally to this work.

https://doi.org/10.1016/j.cclet.2021.07.071
1001-8417/

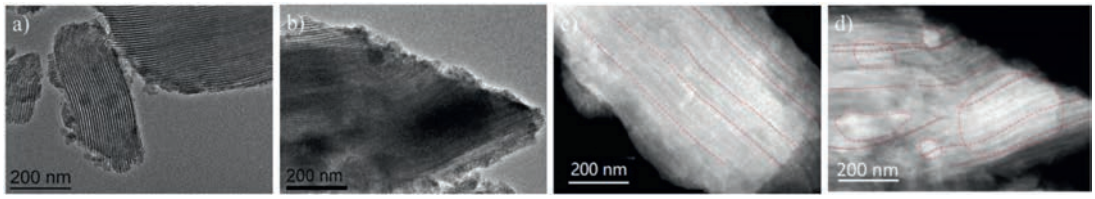

Fig. 1. HRTEM images of (a) $W_{12}Z_{15}$/SBA-15, and (b) W_{12}/Z_{15}/SBA-15. HAADF-STEM images of (c) $W_{12}Z_{15}$/SBA-15 and (d) W_{12}/Z_{15}/SBA-15.

properties and good thermal stability of sulphated zirconia [16–18], but SO_4^{2-} tends to leach in the reaction, resulting in the deactivation of catalysts. Moreover, hierarchical Hβ zeolite and ceria-modified hierarchical Hβ zeolite have been developed as highly efficient solid acid catalysts for alkenylation due to their high thermal stability, while coke is easy to form due to the existence of micropores [19,20]. Therefore, the further work on developing robust alkenylation solid acid catalysts is required.

Tungstated zirconia catalysts have attracted considerable attention in the fields of academia and industry owing to their enhanced regeneration ability and good thermal stability [21], and have been applied to diverse reactions [22–28], but rare reports on alkenylation. Here, we developed highly dispersed silicotungstic acid (STA)-derived WO_3 composited with ZrO_2 supported on SBA-15 (called as WZ/SBA-15) as mesoporous solid acid catalyst prepared by incipient wetness impregnation (IWI) method, that the active components, WO_3 and ZrO_2, were impregnated into the channels of SBA-15 simultaneously to enhance the interaction among them, with a subsequent calcination process for the alkenylation. Besides, alkenylation of *p*-xylene with phenylacetylene was adopted as a model reaction to test the catalytic properties of as-prepared solid acid catalysts. In addition, the effects of the molar ratio of ZrO_2 to WO_3 ($n(ZrO_2/WO_3)$) and calcination temperature (T) on the catalysts performance were investigated as well. High resolution transmission electron microscopy (HRTEM), high-angle annular dark-field scanning transmission electron microscopy (HAADF-STEM), N_2 adsorption-desorption, FT-IR, X-ray diffraction (XRD), X-ray photoelectron spectroscopy (XPS), NH_3 temperature-programmed desorption (NH_3-TPD), and FT-IR of pyridine adsorption (Py-IR) characterization techniques were employed to reveal the relationship between the catalysts' nature and catalytic properties.

The SBA-15 material was prepared according to the procedure described by Zhao [29]. Solid acid catalysts $W_{12}Z_X$/SBA-15-T (X is defined as the molar content of ZrO_2 in contrast to WO_3, X = 12, 15, and 24; T stands for the calcination temperature) were prepared by IWI method by using the mixed aqueous solution containing zirconium nitrate pentahydrate and STA as an impregnant with a subsequent calcination process at a certain temperature for 3 h, and details of preparation process are described in Supporting information. The WO_3-ZrO_2 composite oxide structure of the obtained product is proved by XRD and XPS. Without specific emphasis, $W_{12}Z_X$/SBA-15 stands for the samples calcined at 550 °C. The preparation methods of ZrO_2/SBA-15, WO_3/SBA-15, and W_{12}/Z_{15}/SBA-15 are similar to $W_{12}Z_{15}$/SBA-15 with some changes. Related characterization parameters and details of catalytic performance tests are showed in Supporting information.

Fig. 1 shows the HRTEM and HAADF-STEM images of $W_{12}Z_{15}$/SBA-15 and W_{12}/Z_{15}/SBA-15. Obviously, the ordered mesoporous structure of SBA-15, proved by XRD and N_2 adsorption-desorption, can be seen in both samples after the loading of active ingredients, ZrO_2 and WO_3. Besides, it is clear that no obvious accumulation of large particles can be observed in $W_{12}Z_{15}$/SBA-15, while the phenomenon is serious in W_{12}/Z_{15}/SBA-15. The results obtained above implies the enhanced interaction between ZrO_2 and WO_3 in $W_{12}Z_{15}$/SBA-15, which is in favor of the dispersion of WO_3 in ZrO_2 to produce more acid sites, supported by other characterization results.

Fig. 2a shows the wide XRD patterns of WO_3/SBA-15, ZrO_2/SBA-15, W_{12}/Z_{15}/SBA-15, and $W_{12}Z_{15}$/SBA-15. Obviously, a broad peak at around 2θ = 20°-35°, indicating the amorphous phase of SBA-15 [30], can be observed in all samples. For WO_3/SBA-15, typical diffraction peaks of WO_3 can be observed, meaning that the STA has decomposed into WO_3 due to the high calcination temperature [31–34]. Moreover, no typical diffraction peaks of ZrO_2 in ZrO_2/SBA-15 can be observed, suggesting that ZrO_2 uniformly disperses inside the channels of SBA-15 according to previous reports [35,36]. Noticeably, no obvious peaks attributed to WO_3 and ZrO_2 can be observed in $W_{12}Z_{15}$/SBA-15, evidencing that the impregnation method, that active ingredients, ZrO_2 and WO_3, are impregnated into the channels of SBA-15 simultaneously, achieves the uniform dispersion of WO_3 in ZrO_2, which is derived from the strong interaction in the formed composite oxide WO_3-ZrO_2. Nevertheless, some peaks assigned to WO_3 can be observed in W_{12}/Z_{15}/SBA-15 clearly, and the large grains of WO_3 suggest the uneven dispersion of WO_3 due to the relatively weak interaction between ZrO_2 and WO_3 in contrast to $W_{12}Z_{15}$/SBA-15. The analysis results of XRD are consistent with HRTEM and HAADF-STEM. From the small angle XRD results shown in Fig. S1 (Supporting information), the typical diffraction peaks at 2θ = 0.5°-2° are attributed to the diffraction of the (100), (110) and (200) planes of SBA-15 [37], associated with *P6mm* hexagonal symmetry of SBA-15, which can be observed in $W_{12}Z_{15}$/SBA-15, indicating the preservation of ordered mesoporous structure, being consistent with the analysis results above. N_2 adsorption-desorption isotherms and pore size distributions of the as-prepared catalysts are presented in Fig. 2b, and SBA-15 is introduced as comparison. The specific surface area (S_{BET}) and pore volume (V_{total}) are listed in Table S1 (Supporting information). From Fig. 2b, the characteristic isotherms suggest the mesoporous structure of all the samples. However, the loading of active ingredients results in the remarkable decreases of S_{BET}, V_{total} and pore size in all samples, especially $W_{12}Z_{15}$/SBA-15 and W_{12}/Z_{15}/SBA-15, as shown in Table S1 and Fig 2b. Noticeably, the sharply reduced pore size of WO_3/SBA-15 relative to others indicates the STA tends to aggregate into large particles and evolves into WO_3 after the calcination process at high temperature, resulting in the blockage of channels, which is harmful for mass transfer. Consequently, the increased pore sizes of $W_{12}Z_{15}$/SBA-15 and W_{12}/Z_{15}/SBA-15, especially the former one, in contrast to WO_3/SBA-15, evidences the effect of ZrO_2 on the dispersion of WO_3. Moreover, compared with W_{12}/Z_{15}/SBA-15, $W_{12}Z_{15}$/SBA-15 has larger S_{BET}, V_{total} and pore size, which is favorable for the dispersion of acidic sites and mass transfer. The acidic properties are the crucial factor for the catalytic performance. Thus, NH_3-TPD method was applied to uncover the acid sites nature of the prepared catalysts. NH_3-TPD profiles are presented in Fig. 2c, and the amount of acid sites (N_a) of the as-prepared catalysts is listed in Table S1. The amount of acidic sites in single component solid acid catalysts ZrO_2/SBA-15 is 71.22 μmol/g and WO_3/SBA-15 possesses a few more acid sites, reaching 136.53 μmol/g. For

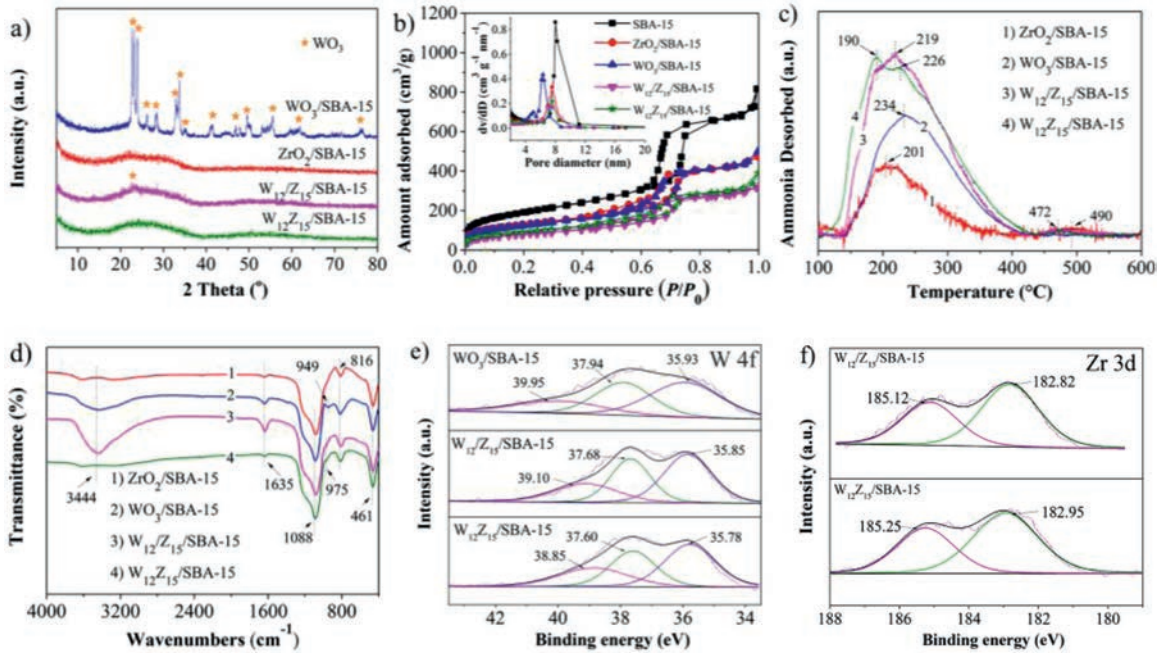

Fig. 2. (a) Wide angle XRD patterns. (b) N_2 adsorption-desorption isotherms (insert: pore size distributions). (c) NH_3-TPD profiles. (d) FT-IR spectra. (e) W 4f and (f) Zr 3d XPS profiles of the prepared catalysts with diverse preparation methods.

W_{12}/Z_{15}/SBA-15, the amount of acid sites is basically equal to the sum of ZrO_2/SBA-15 and WO_3/SBA-15. Surprisingly, the amount of acid sites increased sharply in $W_{12}Z_{15}$SBA-15, reaching to 232.46 μmol/g due to the formation of more composite oxide WO_3-ZrO_2 originated from the special impregnation way of active species described above, which is conductive to enhance solid acidity proved by previous reports [21,38]. The large number of acid sites in $W_{12}Z_{15}$SBA-15 evidences the strong interaction of WO_3 and ZrO_2. Moreover, the acidic properties of $W_{12}Z_{15}$/SBA-15 and W_{12}/Z_{15}/SBA-15 solid acid catalysts were also tested by Py-IR at 150 °C desorption temperature, which can be assigned to total acid sites. As shown in Fig. S2 (Supporting information), the vibration bands at 1540 cm^{-1} and 1450 cm^{-1} are ascribed to the B and L acid sites, respectively. Obviously, both B and L acidic centers can be observed on the two samples, and the L/B acid site on $W_{12}Z_{15}$/SBA-15 is much larger than that on W_{12}/Z_{15}/SBA-15. Combined with NH_3-TPD results, the increased acid sites in $W_{12}Z_{15}$/SBA-15 relative to W_{12}/Z_{15}/SBA-15 are attributed to L acid sites. Both B and L acid sites can promote this reaction according to previous reports [1–3,11,13]. Fig. 2d shows the framework FT-IR spectra of as-prepared solid acid catalysts. All samples display three absorption peaks at 1088, 816 and 461 cm^{-1}, which are attributed to Si-O-Si stretching, Si-O stretching, and Si-O-Si bending modes of vibration in SBA-15, respectively [39–41]. These bands, together with the band at about 3458 cm^{-1} and the band at 1635 cm^{-1} assigned to vibration of the -OH stretching vibration mode and adsorbed water respectively [40,42], can be observed in all samples. In the spectra of ZrO_2/SBA-15, no obvious vibration mode of ZrO_2 can be observed due to overlapping with SBA-15 [43,44]. And for WO_3/SBA-15, the band at 949 cm^{-1} is assigned to the Si-O-W linkage [45–47]. Obviously, the peak intensity of the band reduces sharply and shifts to 975 cm^{-1} in $W_{12}Z_{15}$/SBA-15 and W_{12}/Z_{15}/SBA-15 after the introduction of ZrO_2, evidencing the strong interaction between WO_3 and ZrO_2. Noticeably, the strong absorption peaks of −OH stretching vibration mode and adsorbed water can be observed in WO_3/SBA-15 and W_{12}/Z_{15}/SBA-15, meaning the existence of a considerable amount of water, which is harmful for alkenylation, because the acid sites are easily covered by the water molecules from the competitive adsorption of aromatic compound, resulting in a situation that the aromatic compound are hindered to approach the active centers [48]. The electronic environment of active sites can affect the adsorption properties of reactant [49–52], so the prepared catalysts were investigated by XPS. Fig. 2e shows the XPS spectra of the W 4f region. The peaks at binding energies of 35.93 eV and 37.94 eV in WO_3/SBA-15 can be assigned to W^{6+} species [53–56]. A small peak at ~40 eV is due to W $5P_{3/2}$ [53]. Clearly, these peaks shift to lower region in W_{12}/Z_{15}/SBA-15 and $W_{12}Z_{15}$/SBA-15, implying the strong interaction between WO_3 and ZrO_2, which is further confirmed by the analysis of Zr 3d spectra. The much lower binding energies of W^{6+} species in $W_{12}Z_{15}$/SBA-15 suggest the enhanced interaction between WO_3 and ZrO_2, resulting in the formation of more composite oxide WO_3-ZrO_2. Fig. 2f shows the XPS spectra of Zr 3d region. The binding energies of 182.82 eV and 185.12 eV are assigned to Zr^{4+} species in W_{12}/Z_{15}/SBA-15 [53], which shift to higher region in $W_{12}Z_{15}$/SBA-15 due to the high electron attractor effect of the neighboring W atoms [57], which demonstrates the enhanced interaction between WO_3 and ZrO_2 in contrast to W_{12}/Z_{15}/SBA-15 again. According to the analysis results above, $W_{12}Z_{15}$/SBA-15 prepared by the special impregnation method mentioned above possesses more acid sites, relatively high S_{BET}, large V_{total} and moderate pore size due to the uniform dispersion of WO_3 in ZrO_2 originated from the strong interaction among them, which is in favor of alkenylation.

In order to verify the effect of synergy of WO_3 with ZrO_2 on the boost for the alkenylation of *p*-xylene with phenylacetylene, the catalytic properties of prepared catalysts were investigated and the reaction results are depicted in Table 1. The alkenylation reaction of *p*-xylene with phenylacetylene is a quite complex competition process, and the mixture consists of main product α-(2,5-dimethylphenyl) styrene (**I**), also called as α-arylstyrene, and side-products acetophenone (**II**), α-(2,5-dimethylphenyl)ethylbenzene (**III**), β-(2,5-dimethylphenyl)styrene (**IV**), and oligomers (**V**). From Table 1, $W_{12}Z_{15}$/SBA-15 exhibits the best catalytic performance due to more acid sites, relatively high S_{BET}, large V_{total} and suitable pore size. The conversion of phenylacetylene can reach 94.7% with a

Table 1
Reaction results for the alkenylation of p-xylene with phenylacetylene over prepared catalysts with diverse preparation methods.[a]

Catalysts	Con. (%)	Product distribution (%)				
		I	II	III	IV	V
ZrO_2/SBA-15	56.0	93.3	0.0	0.1	0.4	6.1
WO_3/SBA-15	73.5	75.6	1.2	0.1	17.3	5.8
W_{12}/Z_{15}/SBA-15	79.9	81.5	0.1	0.0	9.0	9.4
$W_{12}Z_{15}$/SBA-15	94.7	88.4	0.0	0.6	6.5	4.4

[a] Reaction conditions: $n_{p\text{-xylene/Phen}}$ = 25:1, T_r = 150 °C, *TOS* = 6 h, P_s = 1.0 MPa, $m_{cat.}$ = 0.8 g, *VHSV* = 7.5 mL h^{-1} $g_{cat.}{}^{-1}$

considerable selectivity of α-arylstyrene, reaching 88.4%. Besides, fewer oligomers (**V**), being easy to evolve into coke during the reaction, can be attained over $W_{12}Z_{15}$/SBA-15 compared with the other three samples, evidencing that the oligomerization is limited and therefore coke reduces, preventing the deactivation of catalysts consequently. However, W_{12}/Z_{15}/SBA-15 presents poorer catalytic properties compared with $W_{12}Z_{15}$/SBA-15, both the conversion of phenylacetylene and the selectivity of α-arylstyrene, due to the relatively weak interaction between WO_3 and ZrO_2. Moreover, the specific activity results shown in Table S2 (Supporting information) suggest that the excellent performance of $W_{12}Z_{15}$/SBA-15 is attributed to the increase of number of active sites and the enhanced intrinsic activity of acid sites, evidencing the superiority of $W_{12}Z_{15}$/SBA-15 again. Not surprisingly, it is anticipated that both ZrO_2/SBA-15 and WO_3/SBA-15 show bad results for the alkenylation, even though ZrO_2/SBA-15 presents considerable α-arylstyrene selectivity, reaching 93.3%. Combined with characterization and reaction results, the enhanced interaction of WO_3 with ZrO_2 in $W_{12}Z_{15}$/SBA-15, contributing to the formation of more composite oxide WO_3-ZrO_2 resulting from the special impregnation way of active component, has a decisive effect on the boost for alkenylation of *p*-xylene with phenylacetylene. Clearly, $W_{12}Z_{15}$/SBA-15 prepared by the method described above is more conducive for alkenylation. Consequently, the composition of active species and the calcination temperature of the solid acid catalysts were optimized to obtain the optimal catalyst.

According to results above, the introduction of ZrO_2 is favorable for the dispersion of WO_3, and the formation of composite oxide WO_3-ZrO_2 can produce more acid sites. Therefore, a series of $W_{12}Z_X$/SBA-15 solid acid catalysts with various $n(ZrO_2/WO_3)$ were prepared. The effect of $n(ZrO_2/WO_3)$ on the catalyst structure was investigated by XRD experiments, and the characterization results are shown in Fig. S3 (Supporting information). Obviously, two weak peaks assigned to WO_3 can be observed in $W_{12}Z_{12}$/SBA-15, not seen in $W_{12}Z_{15}$/SBA-15 and $W_{12}Z_{24}$/SBA-15. Therefore, it is clear that the high loading of ZrO_2 helps to disperse WO_3 through the strong interaction among them. Figs. S4a and b (Supporting information) present N_2 adsorption-desorption isotherms and pore size distributions of the as-prepared $W_{12}Z_X$/SBA-15 catalysts. The S_{BET}, and V_{total} are listed in Table S3 (Supporting information). With the rise of $n(ZrO_2/WO_3)$ from 12/12 to 24/12, the S_{BET} decreases monotonically due to the high loading of active ingredients. Moreover, V_{total} and pore size increase when $n(ZrO_2/WO_3)$ increases from 12/12 to 15/12 due to the more uniform dispersion of WO_3 in ZrO_2 reducing the blockage of channels, resulting from the strong interaction among them. However, smaller V_{total} and pore size can be obtained in $W_{12}Z_{24}$/SBA-15 due to excessive addition of ZrO_2 compared with $W_{12}Z_{15}$/SBA-15, which is harmful for mass transfer. According to the results above, the conclusion can be obtained that the appropriate addition of ZrO_2 is beneficial to the dispersion of WO_3 to form composite oxide WO_3-ZrO_2, which is conductive to produce more accessible acid sites. Nevertheless, excessive addition of ZrO_2 results in the reducing of exposure of composite oxide WO_3-ZrO_2 to surface, fewer accessible acid sites producing consequently confirmed by NH_3-TPD results. Fig. S5 (Supporting information) shows the NH_3-TPD profiles of the as-prepared catalysts, and the number of acid sites is listed in Table S3 (Supporting information). Clearly, $W_{12}Z_{15}$/SBA-15 has the acidest sites due to the appropriate loading of ZrO_2, being consistent with analysis results above. Fig. 3a and Table S4 (Supporting information) shows the catalytic performance of as-prepared $W_{12}Z_X$/SBA-15 catalysts with diverse $n(ZrO_2/WO_3)$. Based on more acid sites, larger V_{total} and pore size compared with the other two samples, $W_{12}Z_{15}$/SBA-15 shows best catalytic performance for alkenylation. Due to the suitable pore size, the least oligomers (**V**) can be obtained over $W_{12}Z_{15}$/SBA-15. According to the results above, $W_{12}Z_{15}$/SBA-15 stands for the optimum composition of ZrO_2 and WO_3.

Subsequently, a series of solid acid catalysts calcined at various *T* were prepared. The textural properties of the as-prepared catalysts were investigated by N_2 adsorption-desorption experiment, and relevant results are illustrated in Figs. S6a and b (Supporting information). S_{BET} and V_{total} are listed in Table S5 (Supporting Information). It is obvious that the S_{BET} decreases monotonically with the rise of *T*. Moreover, V_{total} presents a completely opposite tendency in contrast to S_{BET}. The pore size increases when *T* rises from 450 °C to 500 °C, and it decreases when *T* further increases from 500 °C to 550 °C. Fig. S7 (Supporting information) shows the NH_3-TPD profiles of the as-prepared solid acid catalysts calcined at diverse temperature, and the amount of acid sits of relevant catalysts is listed in Table S5. Clearly, $W_{12}Z_{15}$/SBA-15-500 has the acidest sites due to suitable *T*, reaching 234.75 μmol/g, which is greater than $W_{12}Z_{15}$/SBA-15-550. Fig. S8 (Supporting information) shows the FT-IR spectra of the as-prepared catalysts, and ZrO_2/SBA-15 and WO_3/SBA-15 are introduced as reference. Obviously, for $W_{12}Z_{15}$/SBA-15-450, the intensity of bands at around 1635 cm^{-1} and 3444 cm^{-1} are obviously stronger compared with the other samples, meaning the existence of quantity of crystalline water, which is harmful to alkenylation. Combined with the results above, appropriate *T* of solid acid catalyst can produce more acid sites, and larger V_{total}, which is favorable for alkenylation. As is shown in Fig. 3b and Table S6 (Supporting information), $W_{12}Z_{15}$/SBA-15-500 shows the best catalytic performance with a 99.4% conversion of phenylacetylene and a 92.3% selectivity of α-arylstyrene due to the acidic sites, large V_{total}. Moreover, very low level of oligomers (**V**) can be obtained at the same time, which is attributed that suitable pore size reduces the formation of coke and avoids the blockage of channels, being conductive to mass transfer. Besides, $W_{12}Z_{15}$/SBA-15-450 shows obviously worse catalytic properties compared with the other three samples, resulting from the overlay of active sites by the considerable crystalline water proved by FT-IR. Therefore, the calcination temperature of 500 °C is most favorable for obtaining optimized solid acid catalyst for alkenylation.

In addition, the stability and regeneration of the obtained optimized solid acid catalyst $W_{12}Z_{15}$/SBA-15-500 was investigated, and the conversion and selectivity as a function of time on steam for the alkenylation of *p*-xylene with phenylacetylene over the fresh and regenerated $W_{12}Z_{15}$/SBA-15-500 is shown in Figs. 3c and d, with WO_3/SBA-15 introduced as comparison. At 300 min, $W_{12}Z_{15}$/SBA-15-500 presents the highest conversion of phenylacetylene with the highest selectivity of α-arylstyrene, reaching 99.4% and 92.9% respectively. 77.9% conversion can be maintained for up to 480 min of time on stream over $W_{12}Z_{15}$/SBA-15-500 solid acid catalyst with excellent 91.3% selectivity of α-arylstyrene. Moreover, the selectivity of α-arylstyrene still reaches 87.8% at 720 min with a poor catalytic activity, implying the deactivation of part of catalysts. As for regenerated one, recovered from spent $W_{12}Z_{15}$/SBA-15-500 by a simple calcination process, the activity and selectivity of α-arylstyrene are just a little less than the fresh

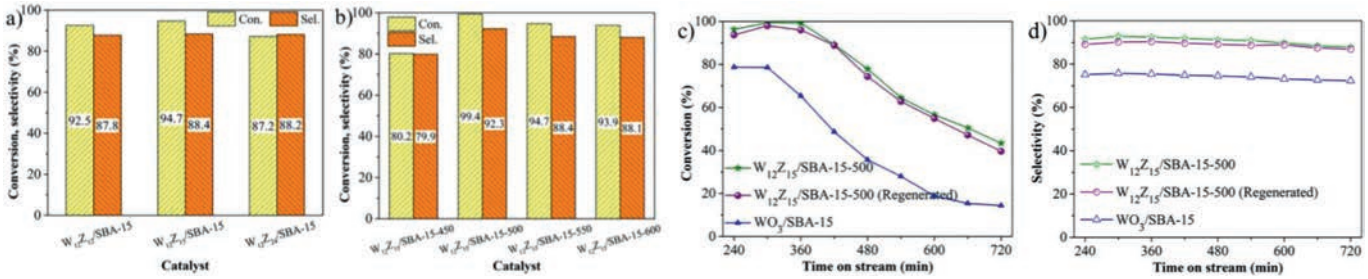

Fig. 3. (a) Reaction results for the alkenylation of *p*-xylene with phenylacetylene over $W_{12}Z_X$/SBA-15 catalysts with diverse $n(ZrO_2/WO_3)$ and (b) Reaction results for the alkenylation of *p*-xylene with phenylacetylene over $W_{12}Z_{15}$/SBA-15-T catalysts with diverse calcination temperature; Reaction conditions: $n_{p\text{-xylene/Phen}}$ = 25:1, T_r = 150 °C, P_s = 1.0 MPa, $m_{cat.}$ = 0.8 g, *VHSV* = 7.5 mL h^{-1} $g_{cat.}{}^{-1}$, *TOS* = 6 h. (c, d) The catalytic stability and regeneration performance of the optimized $W_{12}Z_{15}$/SBA-15-500 solid acid catalyst for the alkenylation of *p*-xylene with phenylacetylene. WO_3/SBA-15 was introduced as comparison.

one with the same variation tendency. It is evident that the deactivation of catalyst is derived from carbon deposition, which can be removed by a simple calcination process. However, the catalytic performance of WO_3/SBA-15 is bad due to more oligomers producing during the reaction, which will evolve into coke to overlay the active sites, resulting in the rapid deactivation of catalyst. According to the evidence described above, $W_{12}Z_{15}$/SBA-15-500 possesses excellent long-time stability and renewability.

In conclusion, the developed ordered mesoporous solid acid catalyst $W_{12}Z_{15}$/SBA-15-500 prepared by IWI method with a subsequent calcination process presents excellent catalytic performance for the alkenylation of *p*-xylene with phenylacetylene, with a 99.4% conversion of phenylacetylene and a 92.3% selectivity of main product (I) α-arylstyrene, which is attributed that the special preparation method that active components, WO_3 and ZrO_2, are impregnated into the channels of SBA-15 simultaneously achieves the uniform dispersion of WO_3 in ZrO_2, resulting in the formation of more composite oxide WO_3-ZrO_2, more accessible acid sites producing consequently. Besides, the relatively high specific surface area, large pore volume and ordered-mesoporous structure of SBA-15 are favorable for mass transfer. Moreover, the regenerated catalyst obtained by a simple calcination process shows comparable catalytic properties with the fresh one, meaning the excellent regeneration of the developed solid acid catalyst. Consequently, $W_{12}Z_{15}$/SBA-15-500 can be regarded as an outstanding candidate for the alkenylation.

Declaration of competing interest

The authors declare that they have no known competing financial interests or personal relationships that could have appeared to influence the work reported in this paper.

Acknowledgments

This work is financially supported by the National Natural Science Foundation of China (No. 21276041) and by the Chinese Ministry of Education *via* the Program for New Century Excellent Talents in University (No. NCET-12-0079).

Supplementary materials

Supplementary material associated with this article can be found, in the online version, at doi:10.1016/j.cclet.2021.07.071.

References

[1] C.E. Song, D. Jung, S.Y. Choung, E.J. Roh, S. Lee, Angew. Chem. Int. Ed. 43 (2004) 6183–6185.
[2] D.S. Choi, J.H. Kim, U.S. Shin, R.R. Deshmukh, C.E. Song, Chem. Commun. 33 (2007) 3482–3484.
[3] K. Komeyama, R. Igawa, K. Takaki, Chem. Commun. 46 (2010) 1748–1750.
[4] C.G. Jia, D.G. Piao, J. Oyamada, et al., Science 287 (2000) 1992–1995.
[5] N.P. Grimster, C. Gauntlett, C.R. Godfrey, M.J. Gaunt, Angew. Chem. Int. Ed. 117 (2005) 3185–3189.
[6] Y. Yamamoto, Chem. Soc. Rev. 43 (2014) 1575–1600.
[7] J.A. Reilly, J.A. Nieuwland, J. Am. Chem. Soc. 50 (1928) 2564.
[8] N. Lucas, A. Bordoloi, A. Amrute, et al., Appl. Catal. A 352 (2009) 74–80.
[9] G. Sartori, F. Bigi, A. Pastorío, et al., Tetrahedron Lett. 36 (1995) 9177–9180.
[10] Z.K. Zhao, Y.T. Dai, T. Bao, R.Z Li, G.R. Wang, J. Catal. 288 (2012) 44–53.
[11] Z.K. Zhao, X.H. Wang, Y.H. Jiao, et al., RSC Adv. 6 (2016) 9072.
[12] Z.K. Zhao, X.H. Wang, Appl. Catal. A 526 (2016) 139–146.
[13] Z.K. Zhao, J.F. Ran, Appl. Catal. A 503 (2015) 77–83.
[14] Z.K. Zhao, J.F. Ran, Y.L. Guo, B.Y. Miao, G.R. Wang, Chin. J. Catal. 37 (2016) 1303–1313.
[15] Z.K. Zhao, Y.L. Guo, Catal. Commun. 93 (2017) 53–56.
[16] M.A. Ecormier, K. Wilson, A.F. Lee, J. Catal. 215 (2003) 57–65.
[17] M.L. Grecea, A.C. Dimian, S. Tanase, V. Subbiah, G. Rothenberg, Catal. Sci. Technol. 2 (2012) 1500–1506.
[18] A.A. Kiss, A.C. Dimian, G. Rothenberg, Adv. Synth. Catal. 348 (2006) 75–81.
[19] Y.L. Guo, Z.K. Zhao, Chem. Eng. Sci. 201 (2019) 25–33.
[20] Y.L. Guo, Y. Zhang, Z.K. Zhao, Chin. J. Catal. 39 (2018) 181–189.
[21] W. Zhou, N. Soultanidis, H. Xu, et al., ACS Catal. 7 (2017) 2181–2198.
[22] F. Chambon, F. Rataboul, C. Pinel, et al., Appl. Catal. A 504 (2015) 664–671.
[23] V.C. dos Santos, K. Wilson, A.F. Lee, S. Nakagaki, Appl. Catal. B 162 (2015) 75–84.
[24] W. Ciptonugroho, M.G. Al-Shaal, J.B. Mensah, R. Palkovits, J. Catal. 340 (2016) 17–29.
[25] W. Lee, C.C. Yang, S. Cheng, J. Chin. Chem. Soc. 68 (2021) 409–420.
[26] M.L. Hernández-Pichardoa, P.D. Angel, J.A. Montoya-de la Fuente, Catal. Today 360 (2021) 72–77.
[27] V.C. Nguyena, A. Dandach, T.T.H. Vub, P. Fongarland, N. Essayem, Mol. Catal. 476 (2019) 110518.
[28] T. Techopittayakul, S. Echaroj, M. Santikunaporn, et al., Reac. Kinet. Mech. Catal. 126 (2019) 529–546.
[29] D.Y. Zhao, J.L. Feng, Q.S. Huo, et al., Science 279 (1998) 548–552.
[30] P. Bhange, D.S. Bhange, S. Pradhan, V. Ramaswamy, Appl. Catal. A 400 (2011) 176–184.
[31] G. Chen, M. Dong, J.F. Li, et al., Catal. Sci. Technol. 6 (2016) 5515.
[32] N. Songsiri, G. Rempel, P. Prasassarakich, Catal. Lett. 149 (2019) 2468–2481.
[33] S. Mohanapriya, S.D. Bhat, A.K. Sahu, et al., Energy Environ. Sci. 3 (2010) 1746–1756.
[34] A.B. Kulala, M.M. Kasabe, P.V. Jadhav, M.K. Dongare, S.B. Umbarkar, Appl. Catal. A 574 (2019) 105–113.
[35] Y. Xie, Y. Tang, Adv. Catal. 37 (1990) 1–43.
[36] X.J. Zhang, J.X. Liu, Y. Jing, Y.C. Xie, Appl. Catal. A 240 (2003) 143–150.
[37] P. Sharma, J. Rathod, A.P. Singh, P. Kumar, Y. Sasson, Catal. Sci. Technol. 8 (2018) 3246–3259.
[38] W. Zhou, E.I. Ross-Medgaarden, W.V. Knowles, et al., Nat. Chem. 1 (2009) 722–728.
[39] D.R. Hua, S.L. Chen, G.M. Yuan, Y.L. Wang, J. Porous Mater. 18 (2011) 729–734.
[40] S.Y. Xing, P.M. Lv, J.Y. Fu, et al., Micropor. Mesopor. Mater. 239 (2017) 316–327.
[41] M.A. Betiha, H.M.A. Hassan, A.M. Al-Sabagh, A.E.R.S. Khder, E.A. Ahmed, J. Mater. Chem. 22 (2012) 17551–17559.
[42] H.X. Gao, Y.F. Huang, X.W. Zhang, et al., Appl. Energy 259 (2020) 114179.
[43] T. Lopez, J. Navarrete, R. Gomez, et al., Appl Catal A 125 (1995) 217–232.
[44] M.M. Ibrahim, H.R. Mahmoud, S.A. El-Molla, Catal. Commun. 122 (2019) 10–15.
[45] C.Y. Chen, H.X. Li, M.E. Davis, Micropor. Mater. 2 (1993) 17.
[46] H. Chen, W.L. Dai, J.F. Deng, K. Fan, Catal. Lett. 81 (2002) 131.
[47] Z.R. Zhang, J.S. Suo, X.M. Zhang, S.B. Li, Appl. Catal. A 179 (1999) 11–19.
[48] C.H. Xu, T. Jin, S.H. Jhung, et al., Catal. Today 111 (2006) 366–372.
[49] L. Fu, R. Wang, C.X. Zhao, et al., Chem. Eng. J. 414 (2021) 128857–128865.
[50] J.H. Yu, C.Z. He, C.Y. Pu, et al., Chin. Chem. Lett. 32 (2021) 3149–3154.
[51] H.Y. Yang, C.Z. He, L. Fu, et al., Chin. Chem. Lett. 32 (2021) 3202–3206.
[52] R. Wang, C.Z. He, W.X. Chen, C.X. Zhao, J.R. Huo, Chin. Chem. Lett. 32 (2021) 3821–3824.

[53] H. Wang, Y.G. Guo, C.R. Chang, et al., Appl. Catal. A 523 (2016) 182–192.
[54] T.Y. Kim, D.S. Park, Y. Choi, et al., J. Mater. Chem. 22 (2012) 10021–10028.
[55] Y.H. Zhang, X.C. Zhao, Y. Wang, et al., J. Mater. Chem. A 1 (2013) 3724–3732.
[56] Y.Q. Fan, S.J. Cheng, H. Wang, et al., Appl. Catal. B 217 (2017) 331–341.
[57] M.A. Cortés-Jácome, C. Angeles-Chavez, E. López-Salinas, et al., Appl. Catal. A 318 (2007) 178–189.